ISSN 1560-0904, Polymer Science, Ser. B, 2015, Vol. 57, No. 3, pp. 257–263. © Pleiades Publishing, Ltd., 2015.

Structural, Morphological, and Electrical Properties of Polyaniline–Fe_2O_3 Nanocomposites[1]

T. Bashir[a], A. Shakoor[a], E. Ahmad[a], M. Saeed[a], N. A. Niaz[a] and S. K. Tirmizi[b]

[a] *Department of Physics Bahauddin Zakariya University Multan, 60800 Pakistan*

[b] *Department of Physics, University of Agriculture Faisal Abad, Pakistan*

e-mail: bashir_tahirphy@yahoo.com

Received January 1, 2015;
Revised Manuscript Received January 23, 2015

Abstract—Nanocomposites of polyaniline with Fe_2O_3 particles have been synthesized by chemical oxidative polymerization method by increasing the weight percentage of Fe_2O_3. The powder X-ray diffraction technique was employed to study the structure and crystallinity of the synthesized nanocomposites. The strong interaction of polyaniline with Fe_2O_3 particles was confirmed using FTIR technique. It was shown that polyaniline is dispersed into Fe_2O_3 particles successfully by in situ polymerization and therefore the degree of crystallinity increased due to crystalline structure of Fe_2O_3 particles. According to SEM and TEM data, most of Fe_2O_3 particles were coated with polyaniline and those nanocomposites have formed a network during the polymerization process as well. Electrical conductivity of polyaniline containing 5 wt % of Fe_2O_3 was higher among all other composites and even than PANI.

DOI: 10.1134/S1560090415030021

INTRODUCTION

Due to the presence of extended π-conjugated system, the intrinsically conducting polymers (ICPs) exhibit conductivity in semiconducting region [1–4]. These materials have great scientific and technological importance due to their unique electrical, electronic, optical, and optoelectronic characteristics [5, 6]. Polyaniline (PANI), polypyrrole, and polythiophene are typical examples of ICPs. In neutral state, these materials exhibit semiconducting or insulating behavior due to the existence of wide energy gap (~2 eV) with low electrical conductivity of around 10^{-10} to 10^{-5} S/cm [3]. These conducting polymers have to be doped to achieve higher conductive states. The doped conducting polymers may have electrical conductivity in the range of 0.1 to 10^4 S/cm for different polymers through redox reaction or protonation [3]. ICPs have a wide range of applications in various fields such as organic light emitting diodes [7–10], polymer/plastic solar cells [11–14], sensors [15–18], electrocatalysis [19], opto-electronic devices [20], EMI shielding and electrostatic charge dissipation [21–26]. However many ICPs have poor mechanical properties, causing hindrance in their processing [27].

Much attention has been paid for the synthesis of conducting polymer composites with metal oxides to possibly tune and optimize their properties by carefully controlling the dopant metal oxides into the polymer matrix [28]. These composite systems can provide new synergistic properties that cannot be attained from individual materials [29–33], such that the conductivity is more easily controlled, and the mechanical or thermal stability is improved through the synthesis of the nanocomposites [34]. In recent years, the development of inorganic/polymer hybrid materials on nanometer scale have been receiving significant attention due to a wide range of potential applications in optoelectronic devices [35–37] and in field effect transistors [38]. The inorganic fillers at nanoscale exhibit high 'surface to volume ratio' and thus are expected to modify drastically the electrical, optical and dielectric properties of the polymer. In general, the synthesis of hybrid polymer/inorganic material has the goal of obtaining a new composite material having synergetic or complementary behaviors between the polymer and inorganic material.

Among various conducting polymers, PANI is unique and promising candidate for potential applications because of its excellent environmental stability and solubility in some organic solvents. PANI has a unique structure due to existence of an alternate arrangement of nitrogen atoms and benzene ring [39]. It is generally recognized to be one of promising conducting polymers for commercial applications due to its several advantageous effects such as; ease of preparation in aqueous medium [40], good stability in air [41], simplicity in doping [42], improved electronic properties [43], electrochromic effects [44], well behaved electrochemical properties [45, 46], moderately high conductivity in doped state [47]. The com-

[1] The article is published in the original.

posites of PANI and magnetic materials like Fe_2O_3 present great fascination because these composites exhibit a wide range of electrical, optical and magnetic properties [48].

Hence, the goal of the present research was to synthesize PANI–Fe_2O_3 composites and to investigate their characteristics by means of various physical and chemical techniques, such as XRD, FTIR, SEM, TEM analysis and temperature dependant DC electrical conductivity.

EXPERIMENTAL

Aniline (Merck) was distilled under reduced pressure and stored at low temperature prior to use. Ammonium persulfate (APS) and Fe_2O_3 (Aldrich) were used as received. All materials were in good analytical grade (AR) form.

The chemical oxidative polymerization of aniline was carried out in HCl solution. To an appropriate amount of distilled aniline (5 g) HCl was added drop wise into polymerization beaker and ensured the total volume of 50 mL. After that, the solution was placed on a magnetic stirrer. 6.125 gram of APS aqueous solution at appropriate concentration was added to the reaction medium. To ensure the thoroughly mixing of materials, the solution was kept continuously stirred for about 3 h. After a period of 24 h, the solution was washed and filtered by double distilled water, until the filtrate become colorless. The product was then dried under vacuum at 70°C. After that, the synthesized PANI was well grinded and finally obtained in the form of fine green powder [49].

For the composite synthesis 5 g of distilled aniline was taken, then 5 mL of HCl was added in aniline drop wise at 0–5°C during 15 min. After that the process was completed and the solution color was altered from dark brown to light brown. On the next step 5 wt % (0.25 g) of Fe_2O_3 was added in the solution and the whole mixture was well stirred for 3 h; 6.125 g of APS was dissolved in 50 mL of cold water ($T < 5$°C) and added to the prepared mixture drop wise by using dropping funnel. This process completed in about 45 min. The stirring was continued for further 2 h to ensure complete polymerization and the final color of mixture was changed to dark green. The same procedure was carried out for a mixture containing 5 g of aniline and 30 wt % (1.5 g) of Fe_2O_3. After ensuring the polymerization, the mixture was filtered and washed with double distilled water until the filtrate became transparent. After filtering, the precipitate was dried under vacuum at 70°C for 24 h. To ensure homogeneity, the dried precipitate was well ground for 1 h using A-grade mortar and pestle, successively washed with acetone prior to grinding. The pallets of the grinded powder were prepared using hydraulic press at pressure of 30 kN for 2 min.

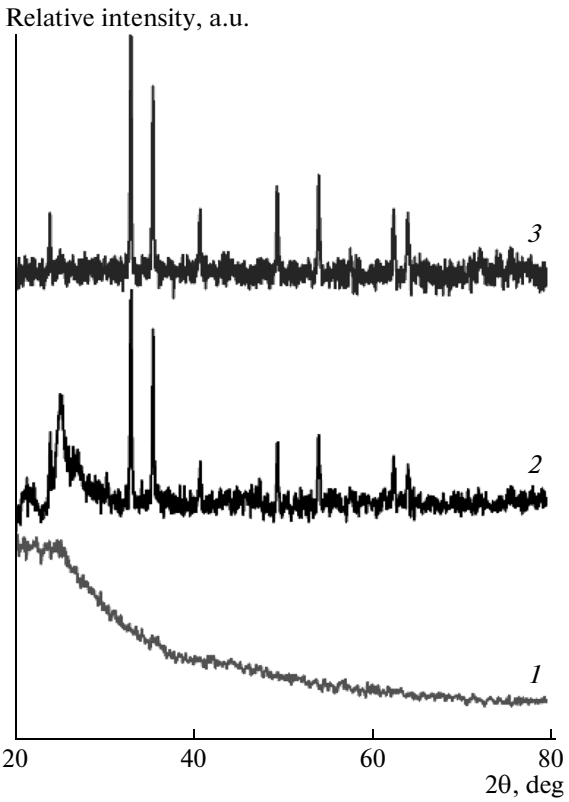

Fig. 1. Diffraction pattern of (*1*) PANI and PANI–Fe_2O_3 composites containing (*2*) 5 and (*3*) 30 wt % of Fe_2O_3.

X-ray powder diffraction (XRD) patterns of the samples were recorded by employing an automated diffractometer Bruker_AXS model D8 using CuK_α radiations ($\lambda = 1.54$ Å). The diffractometer was operated at 40 kV and 50 mA. A scanning step of 0.1° in 2θ with a dwell time of 10 s per step was used.

FTIR spectra were recorded using Perkin-Elmer FTIR spectrometer by KBr pellet method in the region 400 to 4000 cm^{-1}.

The powder morphology of PANI and its composites was investigated using Phillips XL-30 ESEM scanning electron microscope (SEM). The morphology and distribution of Fe_2O_3 nanoparticles were further examined by using Philips CM-200 transmission electron microscope (TEM) operated at 120 kV with a LaB6 filament. The sample preparation for TEM observation was carried out by drying a drop of PANI-Fe_2O_3 nanocomposite powder and ethanol suspension on carbon coated TEM grids.

The temperature dependent DC electrical conductivity studies were performed by using two probe method at temperature range from 293 to 403 K. The samples in the form of pellets having thickness 0.24 cm and diameter 0.83 cm were mounted in a sample holder and connected to a Keithley 2400 electrometer.

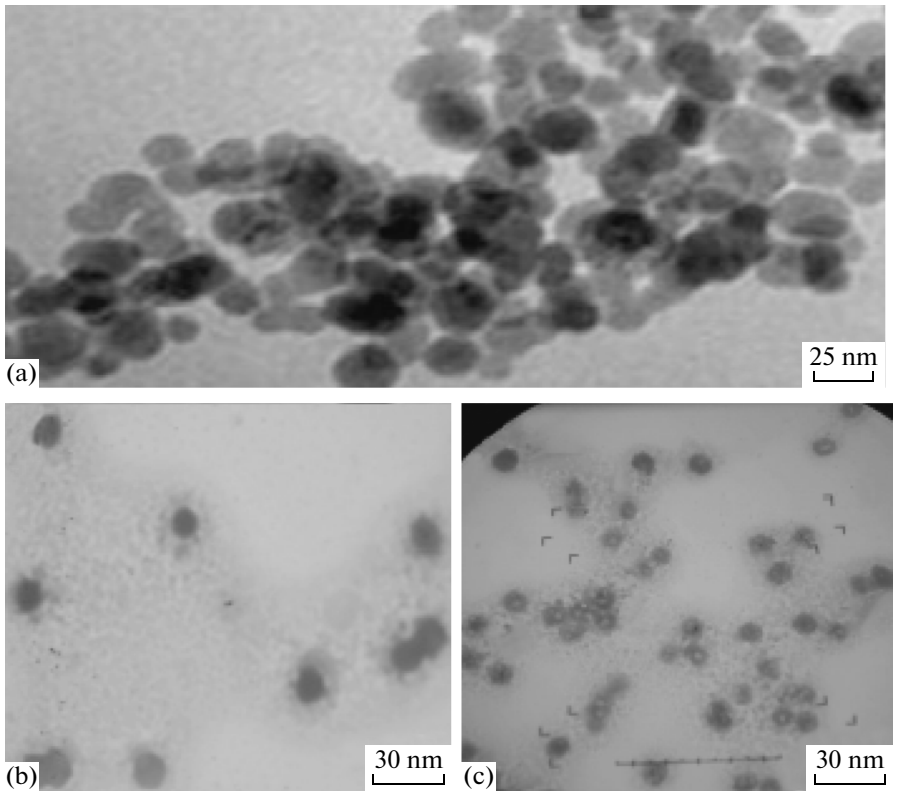

Fig. 2. TEM micrographs of (a) Fe_2O_3 and PANI–Fe_2O_3 composites containing (b) 5 and (c) 30 wt % of Fe_2O_3.

The surrounding temperature of samples was controlled by cryostat and was measured by digital bimetallic thermometer.

RESULTS AND DISCUSSION

A precise comparison of XRD patterns of pure PANI, and PANI composites, which contain 5 and 30 wt % of Fe_2O_3 is shown in Fig. 1. It has been reported previously that the crystallinity of polymers depends on the condition set during the polymer synthesis [49]. The observed spectrum clearly indicates the occurrence of broad peak between $2\theta = 22°$ and 28°, which is due to (110) plane, and it is the characteristic peak of PANI [50]. Thus, it may be concluded that the structure of pure PANI is amorphous as reported in the literature [51]. The pattern of amorphous broad peak (22°–28°) in PANI is present in all PANI–Fe_2O_3 composites according to its proportion. From XRD, intensity versus 2θ graph it is clearly observed that the amorphous nature of PANI is decreasing and crystallinity is increasing with growth of Fe_2O_3 content. Besides, XRD patterns of PANI–Fe_2O_3 composites showed the prominent peaks related to $2\theta = 30.07°$, 35.58°, 49.41°, 56.97° and 62.15° are due to (2 0 0), (3 1 1), (5 1 1), (4 0 0) planes respectively, which are assigned to Fe_2O_3 related peaks [24]. Thus these sharp peaks are clearly showing that after inserting Fe_2O_3 in PANI crystallinity is increased. After careful correspondence, it is evident that Fe_2O_3 retains its character even dispersed in PANI during chemical polymerization. Therefore, this aspect would also be taken into consideration that the composites would also possess ferromagnetic behavior due to the presence of Fe_2O_3 [52]. The detailed discussion on ferromagnetic behavior would be presented in our coming research paper. The average crystallite size of PANI–Fe_2O_3 nanocomposites was calculated by using Scherer's Formula.

$$d = k\lambda/\beta\cos\theta \quad (1)$$

Here d is crystallite size for individual peak, k is the unit cell geometry dependent constant, whose value is typically between 0.85 to 0.99, λ is the wavelength of incident X-ray, β is the full width at half maximum (FWHM) of the peak and θ is the Bragg angle. The average size of Fe_2O_3 nanoparticles and PANI–Fe_2O_3 composites was equal to 25 and 31 nm respectively, which is in good agreement to the results obtained from TEM analysis.

Figure 2 shows the TEM images of Fe_2O_3, PANI–5%Fe_2O_3 and PANI–30%Fe_2O_3 nanocomposites respectively. As is seen from Fig. 2a, the nanoparticles of Fe_2O_3 have not a uniform distribution of shape and seem to be aggregated extensively and have an average size of about 24–28 nm, but when dispersed in PANI (Figs. 2b, 2c) they formed a well oriented regular

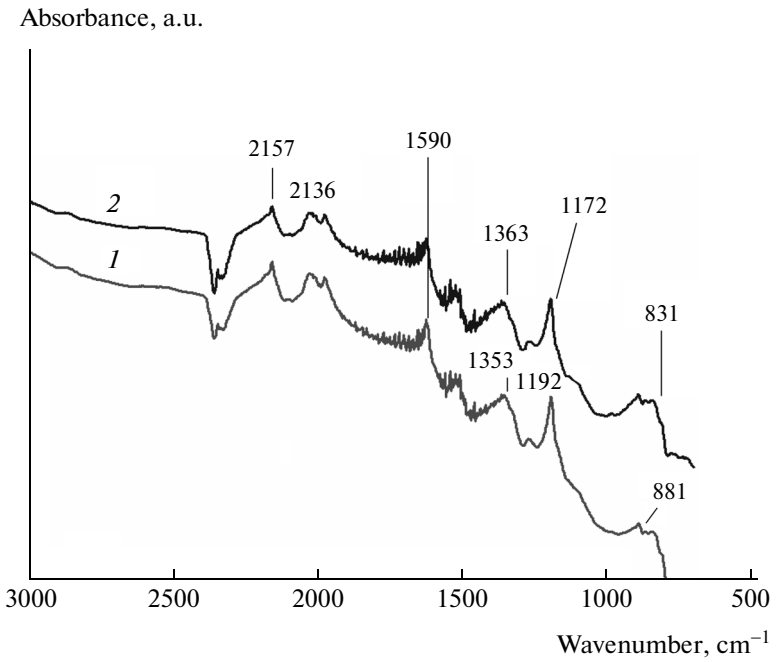

Fig. 3. FTIR spectra of PANI–Fe_2O_3 composites containing (*1*) 5 and (*2*) 30 wt % of Fe_2O_3.

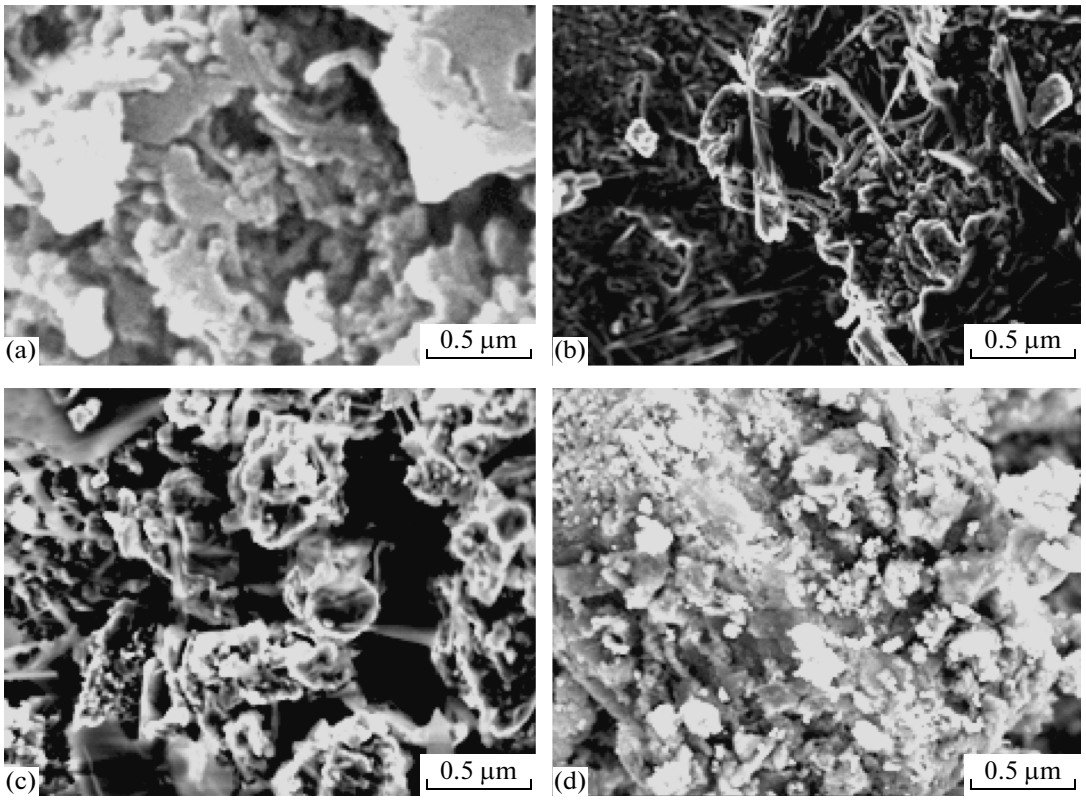

Fig. 4. SEM micrographs of (a) Fe_2O_3, (b) PANI, and PANI–Fe_2O_3 composites containing (c) 5 and (d) 30 wt % of Fe_2O_3.

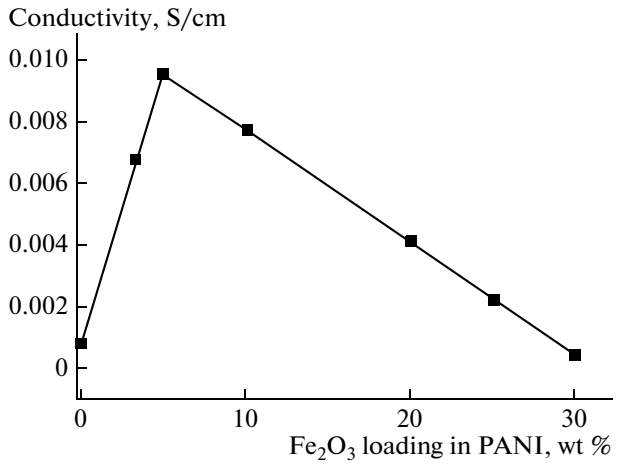

Fig. 5. DC conductivity as a function of Fe_2O_3 loading.

shaped structure with an average size of 29–33 nm. This increase in size may be attributed to the nanoparticles of Fe_2O_3, which are coated with PANI and resulting in increase of nanocomposites size. The same behavior was also reported for PANI/NiO composites [53, 54].

The FTIR spectrum of pure PANI is in agreement with literary data [55], while the absorption spectra of PANI–5%Fe_2O_3 and PANI–30%Fe_2O_3 composites are shown in Fig. 3. The FTIR spectra of the PANI–Fe_2O_3 composites showed bands at 831 and 881 cm^{-1}, which are characteristic peaks of PANI [55]; the spectral band at 1590 cm^{-1} is ascribed as quinone-ring stretching deformation [56]. The spectral bands observed at 1172 cm^{-1} are due to interplane bending of C–H bond and the band observed at 1363 cm^{-1} is due to stretching of C–C bond [57]. While the band observed at 2157 cm^{-1} is due to C–N inter plane bending vibrations [58]. The characteristic peaks of PANI molecules in the composite are shifted to higher wave numbers compared with those of pure PANI. From this, it may reasonably be concluded that there is a strong interaction between PANI and the Fe_2O_3 particles. Moreover, the addition of Fe_2O_3 particles probably results in the formation of hydrogen bonding between the NH proton and an oxygen atom on the Fe_2O_3 surface, which weakens the N–H bond and hence stretching intensity as just in the case of PANI–Y_2O_3 nanocomposites [59, 60].

The SEM image of pure PANI exhibits complete amorphous regions as shown in Fig. 4. This image clearly reveals that surface of PANI is not smooth and uneven lumps and holes are visible, which are suitable for adsorption. It is found that the doping of Fe_2O_3 strongly affected the morphology of the resulting PANI–Fe_2O_3 composite. In case of PANI–Fe_2O_3 composites, a crispy fragmented surface of Fe_2O_3 structure with an interlocking arrangement of granular particles is observed [61]. This suggests that most of Fe_2O_3 particles were coated with PANI and PANI–Fe_2O_3 composites have formed a network during the polymerization process as well. A close investigation suggests that PANI–Fe_2O_3 composites exhibited a porous structure and high surface area [62]. Such porous structure significantly enhances the rapid diffusion and would be advantageous in gas sensing applications [63].

The electrical conductivity of the PANI–Fe_2O_3 composites increases slightly with increasing Fe_2O_3 content and then decreases with excess Fe_2O_3 content as shown in Fig. 5. Similar phenomenon was also described for the nanocomposites of PPY–TiO_2–MMT [64, 65]. The increase in conductivity with Fe_2O_3 contents could be attributed due to alignment and straightening of PANI chains on the surface of Fe_2O_3 particles. At 5 wt % of Fe_2O_3 this alignment and straightening of chains of the polymers become maximum, and as we add more Fe_2O_3 the conductivity decreases due to heterogeneous formation of PANI–Fe_2O_3 composite.

CONCLUSIONS

The chemical oxidative polymerization method was employed for the synthesis of PANI–Fe_2O_3 composites. The crystallinity of synthesized samples was studied by XRD diffraction pattern and it was found to be improved due to crystalline nature of Fe_2O_3 in PANI–F_2O_3 composites. The strong interaction of PANI with Fe_2O_3 particles was confirmed using FTIR. SEM and TEM images of PANI and composites suggest that most of Fe_2O_3 particles were coated with PANI and PANI–Fe_2O_3 composite have formed a network during the polymerization process as well. A marked increase in the conductivity is observed for a critical concentration (5 wt %) of Fe_2O_3, which needs further investigation and in-depth understanding.

ACKNOWLEDGMENTS

Authors gratefully acknowledge the financial support from Bahauddin Zakariya University Multan, Pakistan.

REFERENCES

1. A. P. Singh, A. Chandra, and S. K. Dhawan, AIP Adv. **1**, 022147 (2011).
2. H. Shirakawa, Angew. Chem., Int. Ed. **40**, 2575 (2001).
3. A. G. MacDiarmid, Angew. Chem., Int. Ed. **40**, 2581 (2001).
4. A. J. Heeger, Angew. Chem., Int. Ed. **40**, 2591 (2001).
5. T. A. Skotheim, R. L. Elsenbaumer, and J. R. Reynolds, *Hand Book of Conducting Polymer,* 2nd ed. (Marcel Dekker, New York, 1998).

6. C. J. Brabec, N. S. Sariciftci, and J. C. Hummelen, Adv. Funct. Mater. **11**, 15 (2001).
7. K. Fehse, G. Schwartz, K. Walzer, and K. Leo, J. Appl. Phys. **101**, 124509 (2007).
8. W. H. Kim, A. J. Makinen, N. Nikolov, R. Shashidhar, H. Kim, Z. H. Kafafi, Appl. Phys. Lett. **80**, 3844 (2002).
9. K. Fehse, G. Schwartz, K. Walzer, and K. Leo, J. Appl. Phys. **101**, 124509 (2007).
10. T. Dobbertin, O. Werner, J. Meyer, A. Kammoun, D. Schneider, T. Riedl, E. Becker, H. H. Johannes, W. Kowalsky, Appl. Phys. Lett. **83**, 24 (2003).
11. Y. M. Chang, W.-F. Su, and L. Wang, Macromol. Rapid Commun. **29**, 1303 (2008).
12. J. K. Lee, W. S. Kim, H. J. Lee, W. S. Shin, S. H. Jin, W. K. Lee, M. R. Kim, Polym. Adv. Technol. **17**, 709 (2006).
13. M. Al-Ibrahim, O. Ambacher, S. Sensfuss, and G. Gobsch, Appl. Phys. Lett. **86**, 201120 (2005).
14. C. J. Brabec, N. S. Sariciftci, and J. C. Hummelen, Adv. Funct. Mater. **11**, 15 (2001).
15. H. Yoon, M. Chang, and J. Jang, Adv. Funct. Mater. **17**, 431 (2007).
16. S. Koul, R. Chandra, and S. K. Dhawan, Sens. Actuators, B **75**, 151 (2001).
17. A. D. Aguilar, E. S. Forzani, X. Li, N. Tao, L. A. Nagahara, I. Amlani, R. Tsui, Appl. Phys. Lett. **87**, 193108 (2005).
18. H. Yoon, M. Chang, and J. Jang, Adv. Funct. Mater. **17**, 431 (2007).
19. Z. Weiqiang, D. Yukou, Z. Hongmei, X. Jingkun, Y. Ping, Electrochim. Acta **55**, 2911 (2010).
20. A. Boyel, E. M. Geneis, and M. Lapkowaski, Synth. Met. **28**, 769 (1989).
21. Y. Wang and X. Jing, Polym. Adv. Technol. **16**, 344 (2005).
22. K. Naishadham, IEEE Trans. Electromagn. Compat. **34**, 47 (1992).
23. S. K. Dhawan, N. Singh, and D. Rodrigues, Sci. Technol. Adv. Mater. **4**, 105 (2003).
24. R. Wycisk, R. Pozniak, and A. Pasternak, J. Electrost. **56**, 55 (2002).
25. S. Koul, R. Chandra, and S. K. Dhawan, Polymer **41**, 9305 (2000).
26. Y. Wang and X. Jing, Polym. Adv. Technol. **16**, 344 (2005).
27. Y. Wang, X. Wang, J. Li, J. Mo, X. Zhao, X. Jing, F. Wang, Adv. Mater. **13**, 1582 (2002).
28. N. N. Mallikarjuna, S. K. Manohar, P. V. Kulkarni, A. Venkataraman, T. M. Aminabhavi, J. Appl. Polym. Sci. **97**, 1868 (2005).
29. J. Rong, Z. Jing, H. Li, and M. Sheng, Macromol. Rapid Commun. **22**, 329 (2001).
30. S. T. Lim, Y. H. Hyun, H. J. Choi, and M. Jhon, Chem. Mater. **14**, 1839 (2002).
31. P. Reichert, B. Hoffmann, T. Bock, R. Thomann, R. Mulhaupt, C. Friedric, Macromol. Rapid. Commun. **22**, 519 (2001).
32. X. Tong, H. Zhao, T. Tang, Z. Feng, B. Huang, J. Polym. Sci., Part A: Polym. Chem. **40**, 1706 (2002).
33. S. K. Lim, J. W. Kim, I. Chin, Y. K. Kwon, H. J. Choi, Chem. Mater. **14**, 1989 (2002).
34. J. W. Kim, F. Liu, H. J. Choi, S. H. Hong, J. Joo, Polymer **44**, 289 (2003).
35. B. W. J. E. Beek, L. H. Slooff, M. N. Wienk, J. M. Kroon, R. A. J. Janseen, Adv. Funct. Mater. **15**, 1703 (2005).
36. X. M. Sui, C. L. Shao, and Y. C. Liu, Appl. Phys. Lett. **87**, 113 (2005).
37. D. C. Olson, J. Piris, R. T. Colins, S. E. Shaheen, D. S. Ginley, Thin Solid Films **496**, 26 (2006).
38. J. X. Xu, V. A. L. Roy, P. Stallinga, M. Muccini, S. Toffanin, H. F. Xiang, C. M. Che, Appl. Phys. Lett. **90**, 223 (2007).
39. K. Singha, A. Ohlana, R. K. Kotnalab, A. K. Bakhshic, and S. K. Dhawana, Mater. Chem. Phys. **112**, 651 (2008).
40. P. A. Calvo, J. Rodriguez, H. Grande, D. Mecerreyes, J. A. Pomposo, Synth. Met. **126**, 111 (2002).
41. B. Wesseling, Synth. Met. **4**, 119 (1991).
42. Y. Z. Zheng, K. Levon, T. Taka, J. Laasko, J. E. Osterholm, Polym. J. **28**, 412 (1996).
43. Y. Cao, P. Smith, and A. J. Heeger, PCT Patent Appl. No. WO 92/2291, **91** (1992).
44. Y. Xia, A. G. MacDiarmid, and A. J. Epstein, Macromolecules **27**, 7212 (1994).
45. A. G. MacDiarmid and A. J. Epstein, Synth. Met. **65**, 103 (1994).
46. A. G. MacDiarmid, Y. N. Xia, and J. M. Wiesinger, US Patent No. 5773568 (1998).
47. A. G. MacDiarmid and A. J. Epstein, Synth. Met. **69**, 85 (1995).
48. Y. Sun, G. Guo, B. Yang, W. Cai, Y. Tian, M. He, Y. Liu, Phys. B **406**, 1013 (2011).
49. S. Saravanan, C. J. Mathai, A. R. Anantharaman, S. Venkatachalam, P. V. Prabhakaran, J. Phys. Chem. Solids **67**, 1496 (2006).
50. S. G. Pawar, S. L. Patil, M. A. Chougule, B. T. Raut, D. M. Jundale, V. B. Patil, Arch. Appl. Sci. Res. **2** (2), 194 (2010).
51. A. Shakoor and M. Farooq, Polym. Sci., Ser. A **55** (3), 159 (2013).
52. N. K. Pawar, D. D. Kajale, G. E. Patil, V. G. Wagh, V. B. Gaikwad, M. K. Deore, G. H. Jain, Int. J. Smart Sens. Intell. Syst. **5** (2), 441 (2012).
53. B. I. Nandapure, S. B. Kondawar, M. Y. Salunkhe, and A. I. Nandapure, Adv. Mater. Lett. **4** (2), 134 (2013).
54. Y. Qi, J. Zhang, S. Qiu, L. Sun, F. Xu, M. Zhu, L. Ouyang, D. Sun, J. Therm. Anal. Calorim. **98** (2), 533 (2009).

55. G. D. Prasanna, H. S. Jayanna, Ashok R. Lamani, M. L. Dinesha, C. S. Naveen, G. J. Shankaramurthy, Chin. Phys. Lett. **28** (11), 117701 (2011).
56. I. Bekri-Abbes and E. Srasra, React. Funct. Polym. **70**, 11 (2010).
57. N. Puviarasan, V. Arjunan, and S. M. Turk, J. Chem. **28**, 53 (2004).
58. Infrared Spectroscopy Correlation Table. http://en.wikipedia.org/wiki/Infrared_spectroscopy_ correlation_table.
59. H. S. Xia and Q. Wang, Chem. Mater. **14**, 2158 (2002).
60. E. Kowsari and G. Faraghi, Ultrason. Sonochem. **17**, 718 (2010).
61. I. Ali, A. Shakoor, M. U. Islam, M. Saeed, M. N. Ashiq, M. S. Awan, Curr. Appl. Phys. **13** (6), 1090 (2013).
62. F. Tudorache and M. Grigoras, Optoelectron. Adv. Mater. **4** (1), 43 (2010).
63. R. Khan, P. Khare, B. P. Baruah, A. K. Hazarika, N. C. Dey, Adv. Chem. Eng. Sci. **1**, 37 (2011).
64. A. Shakoor, T. Zahra Rizvi, H. Umer Farooq, N. Hassan, A. Majid, M. Saeed, Polym. Sci., Ser B **53** (9), 540 (2011).
65. A. Shakoor and T. Z. Rizvi, J. Appl. Polym. Sci. **9**, 21 (2009).